Cell Cycle 10:13, 2140-2150; July 1, 2011; © 2011 Landes Bioscience

Scleroderma-like properties of skin from caveolin-1-deficient mice

Implications for new treatment strategies in patients with fibrosis and systemic sclerosis

Remedios Castello-Cros,[1,2,*] Diana Whitaker-Menezes,[1,2] Alex Molchansky,[1,2] George Purkins,[1,4] Louis J. Soslowsky,[5] David P. Beason,[5] Federica Sotgia,[1,2] Renato V. Iozzo[1,4,*] and Michael P. Lisanti[1-3,*]

[1]The Jefferson Stem Cell Biology and Regenerative Medicine Center; [2]Departments of Stem Cell Biology and Regenerative Medicine and Cancer Biology; [3]Department of Medical Oncology; Kimmel Cancer Center; [4]Department of Pathology, Anatomy and Cell Biology; Thomas Jefferson University; [5]McKay Orthopaedic Research Laboratory, University of Pennsylvania; Philadelphia, PA USA

Key words: caveolin-1, skin, scleroderma, systemic sclerosis, fibrosis, preclinical model, metabolism, matrix, autophagy, mitophagy

Abbreviations: Cav-1, caveolin-1; KO, knockout; WT, wild-type

Caveolin-1 (Cav-1), the principal structural component of caveolae, participates in the pathogenesis of several fibrotic diseases, including systemic sclerosis (SSc). Interestingly, affected skin and lung samples from patients with SSc show reduced levels of Cav-1, as compared to normal skin. In addition, restoration of Cav-1 function in skin fibroblasts from SSc patients reversed their pro-fibrotic phenotype. Here, we further investigated whether Cav-1 mice are a useful pre-clinical model for studying the pathogenesis of SSc. For this purpose, we performed quantitative transmission electron microscopy, as well as biochemical, biomechanical, and immuno-histochemical analysis, of the skin from Cav-1$^{-/-}$ null mice. Using these complementary approaches, we now show that skin from Cav-1 null mice exhibits many of the same characteristics as SSc skin from patients. These changes include a decrease in collagen fiber diameter, increased maximum stress (a measure tensile strength) and modulus (a measure of stiffness), as well as mononuclear cell infiltration. Furthermore, an increase in autophagy/mitophagy was observed in the stromal cells of the dermis from Cav-1$^{-/-}$ mice. These findings suggest that changes in cellular energy metabolism (e.g., a shift towards aerobic glycolysis) in these stromal cells may provide a survival mechanism in this "hostile" or pro-inflammatory microenvironment. Taken together, our results demonstrate that Cav-1$^{-/-}$ mice are a valuable new pre-clinical model for studying scleroderma. Most importantly, our results suggest that inhibition of autophagy and/or aerobic glycolysis may represent a new promising therapeutic strategy for halting fibrosis in SSc patients. Finally, Cav-1$^{-/-}$ mice are also a pre-clinical model for a "lethal" tumor micro-environment, possibly explaining the link between fibrosis, tumor progression and cancer metastasis.

Introduction

Systemic sclerosis (SSc) is an auto-immune disease of unknown origin, involving the connective tissue of the skin and multiple internal organs, resulting in high morbidity and mortality.[1] Its pathogenesis is complex and poorly-understood. The hallmark feature of SSc is the excessive production and accumulation of collagen and other extacellular matrix (ECM) proteins, resulting in a thickening of the skin and fibrosis of the affected organs.[1] The excessive collagen deposition in SSc is due to the over-production of this protein by fibroblasts.[2-4] SSc fibroblasts display an activated phenotype, characterized by the increased transcription of genes encoding various collagens and other ECM proteins, the expression of alpha smooth muscle actin (α-SMA) and reduced ECM proteolytic activity.[5,6] Indeed, it is the over-production of collagen by SSc fibroblasts that distinguishes controlled repair, such as that occurring during normal wound healing, from uncontrolled fibrosis.[7]

In tandem with the exaggerated production and accumulation of collagen in skin from SSc patients, altered collagen ultrastructure and biomechanical properties are also apparent. Fibrotic tissues exhibit an accumulation of irregular collagen fibrils of a smaller diameter.[8,9] It is generally accepted that the overall organization, content and physical properties of the collagen fibril network correlates directly with skin strength.[10,11] Indeed, the tensile strength of the skin from SSc patients is substantially increased, as compared to normal skin.[12]

In addition to the excessive deposition of collagen and other ECM components, SSc is also characterized by prominent and

*Correspondence to: Remedios Castello-Cros, Renato V. Iozzo and Michael P. Lisanti
Email: remedios.castello@jefferson.edu, iozzo@mail.jci.tju.edu and michael.lisanti@kimmelcancercenter.org
Submitted: 04/21/11; Accepted: 04/29/11
DOI: 10.4161/cc.10.13.16227

often severe alterations in the microvasculature, and humoral and cellular immunologic abnormalities.[1] The microvasculature of SSc patients displays intimal proliferation and sub-endothelial fibrosis, resulting in frequent narrowing or obliteration of small vessels. Chronic inflammation often occurs in the early stages of SSc and is characterized by infiltration with mononuclear cells. Among the mononuclear cells, macrophages and mast cells are present in large numbers in the clinically involved skin[13,14] and they have been suggested to play a major role in the pathogenesis of scleroderma.

Caveolae are 50 to 100 nm plasma membrane invaginations that represent a morphologically identifiable subset of lipid rafts.[15] The caveolin proteins (caveolin-1, -2 and -3) are the structural components of these organelles. Among them, caveolin-1 (Cav-1) is the best characterized, and it is considered a multi-functional scaffolding protein that recruits and modulates the activity of numerous signaling molecules within caveolae.[16] There is mounting evidence suggesting that Cav-1 participates in the pathology of fibrosis. Cav-1 null mice display a marked increase in extracellular matrix in the lungs and skin, as compared to wild-type mice.[17-19] Tourkina et al. demonstrated that Cav-1 downregulation increases ~5-fold the collagen expression in normal human lung fibroblasts in vitro, whereas overexpression of Cav-1 resulted in a reduction of collagen production. Wang et al.[21] described a significant reduction in Cav-1 levels in lung tissues and fibroblasts from patients with idiopathic pulmonary fibrosis (IPF), as compared with normal controls. Moreover, induction of Cav-1 expression ameliorated bleomycin-induced pulmonary fibrosis and abrogated the TGFβ-induced stimulation of ECM production in the IPF fibroblasts.

Our laboratory previously reported that Cav-1 is markedly decreased in the affected tissues (lungs and skin) and in dermal fibroblasts isolated from SSc patients.[19] Furthermore, murine Cav-1$^{-/-}$ deficient skin fibroblasts display a pro-fibrotic phenotype, and restoration of Cav-1 function in SSc dermal fibroblasts in vitro caused a marked reduction of their collagen expression and inhibited the activity of TGFbeta signaling. Furthermore, we have recently identified that the major signaling pathways activated in Cav-1$^{-/-}$ bone marrow-derived stromal cells, include ROS production, as well as HIF1α and NFκB-activation.[22] These signaling pathways have been implicated in the pathogenesis of multiple pro-fibrotic diseases, including scleroderma.[23,24]

These findings highlight the importance of a loss of Cav-1 in promoting fibrotic disease, in particular in SSc. Here, we show that skin from Cav-1$^{-/-}$ mice recapitulates many of the same alterations observed in the skin of SSc patients, such as fibrotic, vascular and immune processes.

These results suggest that Cav-1$^{-/-}$ mice are a valuable new pre-clinical model for studying the pathogenesis of SSc. Similarly, Cav-1$^{-/-}$ mice are also a pre-clinical model for a "lethal" tumor micro-environment, possibly explaining the link between fibrosis, tumor progression and cancer cell metastasis.[25]

Results

Cav-1$^{-/-}$ mice display abnormal collagen ultrastructure. First, we asked whether murine skin lacking Cav-1 exhibits abnormal collagen ultrastructure, as observed in scleroderma.[9] For this purpose, the dorsal skin from wild-type and Cav-1$^{-/-}$ mice was dissected and skin collagen was examined by quantitative transmission electron microscopy. Using this ultrastructural analysis, we found striking differences between the two genotypes. Specifically, dermal collagen fibers were smaller and more uniform in Cav-1$^{-/-}$ mice, as compared to their wild-type mice counterparts (matched for age and sex) (**Fig. 1A and B**).

To automatically measure the diameter of collagen fibrils, we developed an algorithm using the NIH Image J software (**Sup. Fig. 1**). This computer program was able to eliminate the images out of focus or the staining artifacts and automatically measured the diameter of collagen fibrils, providing an accurate and unbiased determination of the particle density. Using this approach, we observed that both the mean and the median diameters of dermal collagen were significantly ($p < 0.001$) reduced in Cav-1$^{-/-}$ mice (**Fig. 1D**), as compared to wild-type mice (**Fig. 1C**) (42.8 vs. 53.9 nm and 42 vs. 53 nm, respectively). In addition, skin from Cav-1$^{-/-}$ mice also displayed a more uniform collagen fibril diameter distribution range (8–86 nm) than normal skin (11–156 nm). We performed a similar study using tendon and found that the changes were much less striking although the median fiber diameter of the Cav-1$^{-/-}$ animals (n = 1,353) was still significantly smaller ($p = 0.03$), as compared to wild-type controls (n = 1,446) (**Sup. Fig. 2**). Thus, these results indicate that the overall structure of collagen is specifically changed in the dermis of Cav-1$^{-/-}$ animals.

Cav-1$^{-/-}$ mice display increased dermal collagen density. We noticed that the Cav-1$^{-/-}$ animal collagen fibers were more tightly packed than controls and, thus, hypothesized that the collagen density was changed. To determine the collagen density, the number of collagen fibers per unit area were quantified using the aforementioned algorithm (**Sup. Fig. 1**). We found that the collagen density in the Cav-1$^{-/-}$ animals was ~51% greater than wild-type animals (115 vs. 73 fibers/μm^2, $p < 0.001$, **Fig. 2A**). These results are consistent with the previous study of Del Galdo et al.[19] where the authors showed that skin from Cav-1$^{-/-}$ mice exhibits an increased thickness, accompanied by a higher collagen content than normal skin, using the Masson's Trichrome staining and hydroxy-proline assays. No significant differences were found in the fiber density in tendon between the two groups (data not shown).

To further analyze the accumulation and organization of dermal collagen, we stained paraffin embedded skin sections from wild-type and Cav-1$^{-/-}$ mice with picrosirius red. Using this staining, highly cross-linked ("mature") collagen fibers give a strong red birefringence, when observed through a polarized lens. In contrast, less cross-linked (more immature) collagen fibers display a weak yellow/green birefringence. Both wild-type and Cav-1$^{-/-}$ dermal collagen gave a strong red birefringence after staining with picrosirius red, indicating similar degree of collagen cross-linking in both groups. Interestingly, Cav-1$^{-/-}$ mice displayed an increased accumulation of dermal collagen fibers stained with picrosiruis than wild-type mice (**Fig. 2B and C**), this observation also extended to the deeper dermis around skin appendages and blood vessels (**Fig. 2D and E**). Taken together,

these results indicate that collagen density is increased in the dermis of Cav-1$^{-/-}$ animals.

Skin from Cav-1$^{-/-}$ mice shows increased tensile strength and elastic modulus. Previous studies have demonstrated that the overall organization, content and physical properties of the collagen fibril network correlate directly with skin strength.[10,11,31] Tensile tests were performed to investigate whether the differences in collagen density and diameter had an effect on the biomechanical properties of Cav-1$^{-/-}$ murine skin. The maximum stress or tensile strength is the maximum load or force (N) that the skin can be subjected to before failure divided by the initial cross-sectional area (mm^2) of the specimen. Notably, Cav-1$^{-/-}$ skin was significantly more resistant to stress, as compared to wild-type (**Fig. 3A**). Indeed, in similar cross-sectional areas (**Fig. 3B**), the maximal stress measured in MPa was significantly higher in the Cav-1$^{-/-}$ animals than in wild-type (2.16 ± 0.54 vs. 1.35 ± 0.46 MPa, p = 0.017) (**Fig. 3C**). All specimens failed within the gauge length (5 mice each group).

We further evaluated the amount of stress in the skin for a given percent elastic deformation, using the Young's modulus (a measure of "stiffness"). Skin from Cav-1$^{-/-}$ mice was found to exhibit significantly higher modulus than normal skin (9.58 ± 2.75 vs. 5.92 ± 2.59 MPa, p = 0.031). These results indicate that skin from Cav-1$^{-/-}$ mice displays an increased tensile strength and elastic modulus.

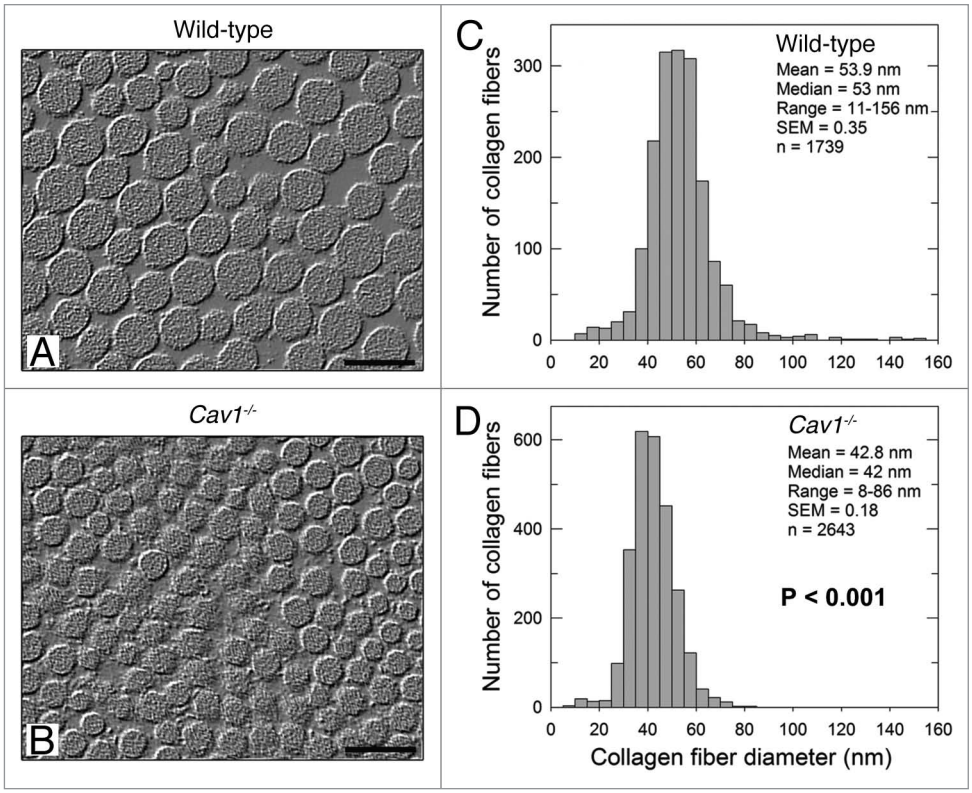

Figure 1. Ultrastructural analysis of the skin from wild-type and Cav-1$^{-/-}$ mice. (A and B) Transmission electron microscopy (EM) micrographs of dermal collagen from wild-type (A) and Cav-1$^{-/-}$ (B) mice. (C and D) Distribution of diameters from dermal collagen from wild-type (C) and Cav-1$^{-/-}$ (D) mice. An Image J algorithm was designed to automatically obtain collagen fiber diameters from EM images (**Sup. Fig. 1**). Using this algorithm, the diameter of 1739 and 2643 collagen fibers was determined from wild-type and Cav-1$^{-/-}$ mice, respectively. Note that dermal collagen from Cav-1$^{-/-}$ mice exhibited a more compact and uniform pattern of fibril diameter and distribution, than wild-type. Indeed the mean and the median collagen diameters from Cav-1$^{-/-}$ mice were significantly smaller than those from wild-type mice ($p < 0.001$, as determined by Mann-Whitney Rank Sum Test using SigmaPlot). Scale bar = 100 nm.

Skin from Cav-1$^{-/-}$ mice displays a net collagen imbalance. We hypothesized that the increased density of dermal collagen in Cav-1$^{-/-}$ mice may be the result of an imbalance between collagen synthesis and degradation. To test this hypothesis, the expression of proly 4-hydroxylase (P4HB) was assessed by immuno-histochemical analysis. P4HB is a key enzyme in collagen biosynthesis, catalyzing the 4-hydroxylation of the prolyl-residues of collagen. The activity of this enzyme generally positively correlates with the rate of collagen synthesis, and its expression has been found to be elevated in scleroderma patients.[32] We observed that the dermis from Cav-1$^{-/-}$ mice exhibits an increased number of P4HB positive cells, when compared to dermis from wild-type mice (**Fig. 4A and B**). Interestingly, the P4HB positive cells in Cav1$^{-/-}$ mice express higher levels of this enzyme, than those positive cells from normal skin. To evaluate collagen degradation activity in the skin, we imaged the degradation of a dense-quench (DQ) fluorogenic collagen type I substrate in the skin from both genotypes. Skin frozen sections were incubated with DQ-Collagen Type I (previously dissolved in LGT-agarose) overnight at RT. The next day, FITC-fluorescence due to collagen degradation was visualized with a confocal microscope. Collagen degradation was observed in the dermis (d), hair follicles (h) and stromal cells (s) (**Fig. 4C and D**). Low or undetectable auto-fluorescence was observed when sections were incubated with LGT-agarose in the absence of DQ-Collagen type I (data not shown). Similar levels of fluorescence and therefore collagen degradation were observed in both groups (**Fig. 4C and D**). These results suggest that the increased dermal collagen density observed in Cav-1$^{-/-}$ mice may be the result of a shift in the synthesis/degradation balance towards a net collagen synthesis.

Skin from Cav-1$^{-/-}$ mice shows the accumulation of myofibroblasts and fibronectin. The overproduction of ECM proteins in scleroderma is mainly mediated by fibroblasts. In particular, it has been suggested that myofibroblasts (activated fibroblasts), which play an active role in collagen biosynthesis, contribute to the pathogenesis of fibrosis.[6] To evaluate the accumulation of myo-fibroblasts in the dermis of wild-type and Cav-1$^{-/-}$ mice, an

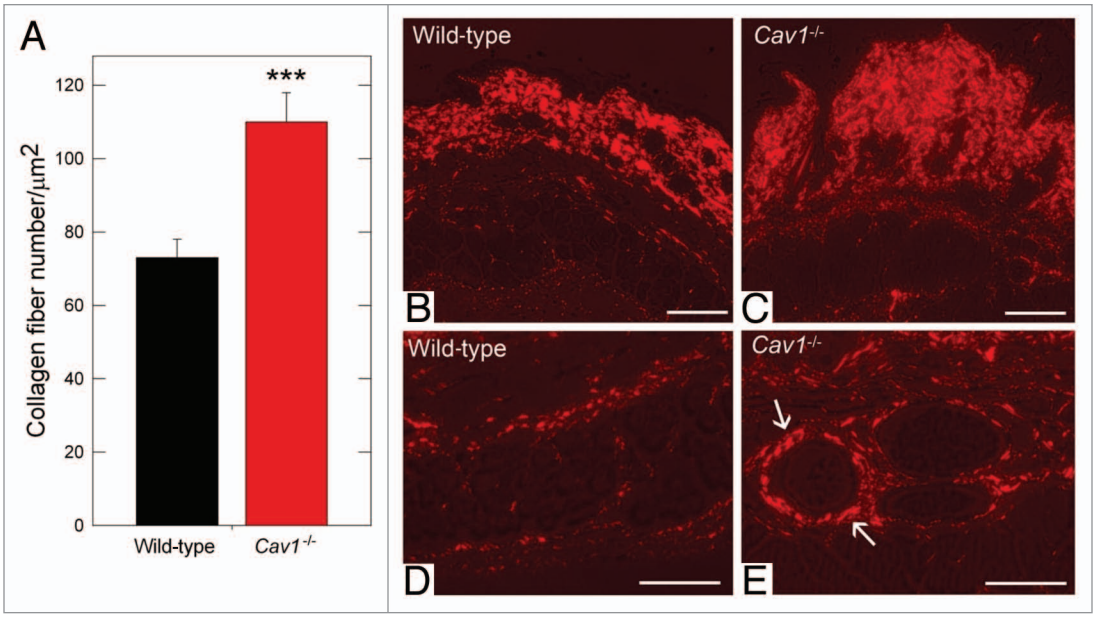

Figure 2. Quantification of dermal collagen density in wild-type and Cav-1$^{-/-}$ mice. (A) Electron microscopy (EM) images of dermal collagen from wild-type and Cav-1$^{-/-}$ mice were analyzed with a custom Image J algorithm (**Sup. Fig. 1**). Using this approach, we determined the collagen density, as number of fibers per unit area. We observed that Cav-1$^{-/-}$ mice contain a significantly larger number of dermal collagen fibrils per unit area, than wild-type animals. (***p < 0.001, as determined by Mann-Whitney Rank Sum Test using SigmaPlot). (B–E) Picrosirius red staining of skin from wild-type and Cav-1$^{-/-}$ mice. Polarized light images of the dermis and the deeper dermis around skin appendages and blood vessels of wild-type (B and D) and Cav-1$^{-/-}$ mice (C and E) were stained with picrosirius red. Mature collagen fibers stained with picrosirius dye appear red when observed under polarized light, whereas less mature fibers, with fewer cross-links, appear yellow and green. Note that although both groups display mature collagen fibers in the dermis, a larger amount of collagen accumulation was found in the dermis, the deeper dermis, and around blood vessels of Cav-1$^{-/-}$ skin, as compared to wild-type mice. Scale bar = 200 µm.

immunohistochemical analysis for alpha-smooth muscle actin (α-SMA), a myo-fibroblast cell marker, was performed in several histological sections from three mice per group. In normal and Cav-1$^{-/-}$ skin, α-SMA was observed surrounding the vessels and in erector pili muscles (data not shown) and in the myo-fibroblasts. Cav-1$^{-/-}$ mice contain an accumulation of α-SMA-positive cells in the dermis, as compared to wild-type animals (**Fig. 5A and B**). In addition to collagen, myo-fibroblasts overexpress other ECM proteins that contribute to fibrosis in scleroderma, including fibronectin, which is highly expressed by fibroblasts isolated from the dermis of scleroderma patients.[33,34] To compare the expression of fibronectin in wild-type and Cav-1$^{-/-}$ mice, total proteins were extracted from four mice per group and the expression of this ECM protein was examined by western blot. Notably, skin from Cav-1$^{-/-}$ mice exhibited increased expression of fibronectin than normal skin (**Fig. 5C**). Indeed, we found that skin from Cav-1$^{-/-}$ mice contained twice the amount of fibronectin, as compared to skin from wild-type mice (1.3 ± 0.13 vs. 0.6 ± 0.06, p = 0.003) (**Fig. 5D**). We also performed immuno-histochemical analysis of fibronectin in skin sections from both groups and we observed increased expression of this ECM protein in the dermis of Cav-1$^{-/-}$ mice (data not shown). Taken together, these data suggests that Cav-1$^{-/-}$ mice display an increased number of myo-fibroblasts that may be responsible for the elevated expression of ECM proteins, such as collagen and fibronectin.

Increased dermal infiltration with macrophages in Cav-1$^{-/-}$ mice. In addition to increased fibrosis, scleroderma is also characterized by dermal infiltration with inflammatory cells.[1] To characterize the degree of inflammatory cell infiltration, we performed immuno-histochemical analysis for F4/80, a macrophage cell marker, in multiples histological sections from three mice per group. Using this approach, we observed that the dermis of Cav-1$^{-/-}$ mice exhibited an increased content of F4/80 positive cells, as compared to dermis from wild-type mice (**Fig. 6A and B**). These data indicate that the dermis from Cav-1$^{-/-}$ mice shows increased infiltration with macrophages. Similar results were also obtained with mast cells, consistent with a generalized pro-inflammatory phenotype (**Fig. 6C–E**).

The dermis of Cav-1$^{-/-}$ mice exhibits increased autophagy/mitophagy activity. Next, we tested whether stromal cells from the dermis of Cav-1$^{-/-}$ mice exhibit an increase in autophagy/mitophagy, as observed in the mammary glands of these mice. To investigate this hypothesis, we evaluated the expression of LC3, an autophagic marker. We observed that the dermis of Cav-1$^{-/-}$ mice exhibits an increase number of autophagic cells (**Fig. 7A and B**). We further analyzed the degree of mitophagy in the dermis of stromal cells from these mice, using BNIP3L, a mitophagy marker. Strikingly almost all the stromal cells from the dermis Cav-1$^{-/-}$ mice are mitophagic, whereas much fewer dermal stromal cells of wild-type mice exhibited mitophagy (**Fig. 7C and D**).

Taken together, these data indicate that stromal cells from Cav-1$^{-/-}$ mice are more autophagic/mitophagic, than wild-type mice.

Discussion

Systemic sclerosis (SSc) is a rare connective tissue disease characterized by increased collagen, abnormal blood vessels and an inflammatory infiltrate. Previous studies strongly suggest that Cav-1 participates in the pathogenesis of fibrotic diseases, such as SSc.[19-21,35] Here, we support these findings and provide new evidence that the skin from Cav-1 null mice recapitulates many of the characteristics of skin from SSc patients, suggesting that Cav-1 null mice may be a new pre-clinical model for understanding SSc.

To determine whether skin from Cav-1$^{-/-}$ mice exhibits abnormal collagen ultrastructure as observed in the skin from SSc patients, we analyzed the status of skin collagen from Cav-1$^{-/-}$ mice by quantitative transmission electron microscopy. We found that the collagen fibril diameter was markedly decreased in Cav-1$^{-/-}$ mice, as compared with control mice. Similarly, previous studies have reported that SSc patients exhibit increased numbers of collagen fibrils, with diameters smaller than those found in normal adult skin.[9,36,37] These smaller diameter fibers possess morphologic characteristics typical of embryonic collagen.[36] Therefore, it has been suggested that these collagen fibrils, with reduced diameters, are a consequence of an increased rate of collagen synthesis. In agreement with this idea, we found a marked increase in the expression of P4HB, prolyl 4-hydroxylase, in the dermis of Cav-1$^{-/-}$ mice. P4HB is a key enzyme in collagen biosynthesis, and this enzyme (through the 4-hydroxylation of prolyl residues) confers thermal stability of collagen triple helix.[38] In addition, P4HB also acts as a chaperone preventing the release of unfolded pro-collagen chains from the endoplasmic reticulum.[39] The level of P4HB activity positively correlates with the rate of collagen biosynthesis, and it has been suggested to contribute signficantly to the development of fibrosis. Indeed, the activity of this enzyme has been found to be increased in SSc fibroblasts, as well as in skin from patients with scleroderma and/or other connective tissue syndromes.[32,40-42]

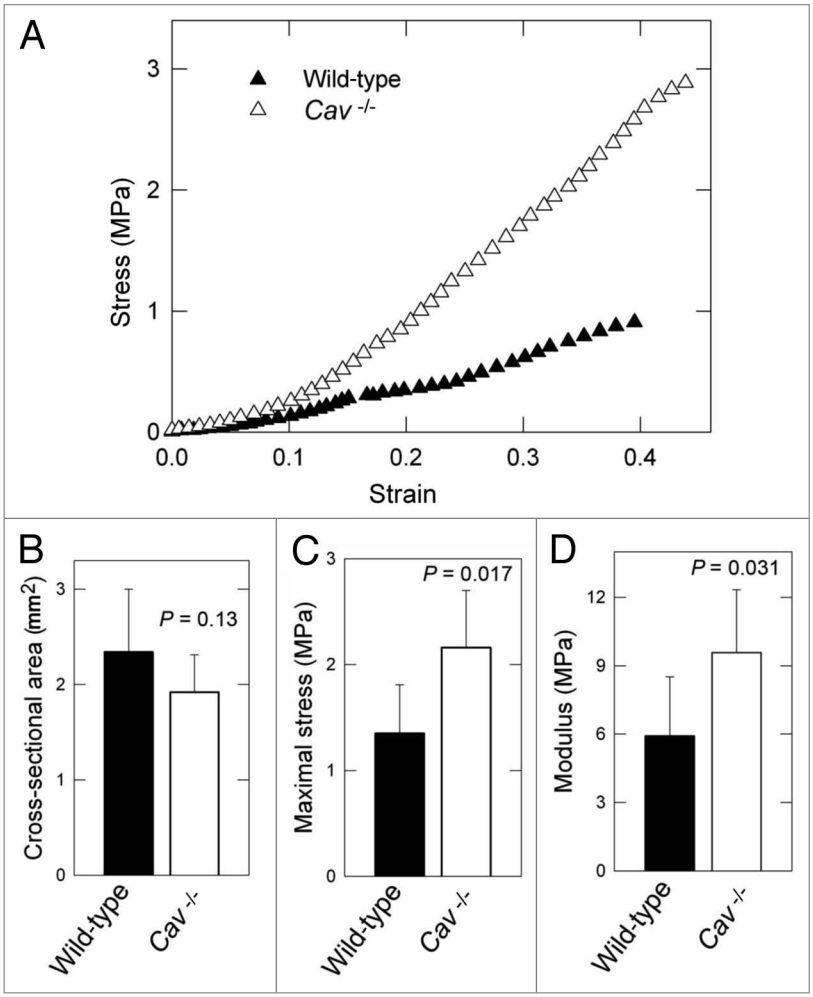

Figure 3. Bio-mechanical properties of the skin from wild-type and Cav-1$^{-/-}$ mice. (A) Typical stress-strain response for wild-type versus Cav-1$^{-/-}$ dorsal skin. (B) No differences were found in the cross-sectional area between the two groups. (C and D) Determination of tensile strength and modulus in the skin in wild-type and Cav-1$^{-/-}$ mice. The maximum stress or "tensile strength" is the maximum amount of tensile stress that a body can be subjected to before failure and Young's modulus (slope of elastic region) is related to "stiffness," the resistance of the material to elastic percent deformation caused by an applied stress. Skin from Cav-1$^{-/-}$ mice exhibited increased maximum stress (C) and modulus (D), than those from wild-type (C and D). Five animals of each genotype were analyzed. Data are reported as the mean ± SEM (p values are indicated in the graphs, as determined by the Student's t-test).

A clear hallmark of SSc is the exacerbated deposition and accumulation of collagen and other ECM proteins. Interestingly, Del Galdo et al.[19] reported that skin biopsies from Cav-1 null mice showed an increase in dermal thickness, accompanied by an ~2.5 fold increase in the content of collagen, as analyzed by hydroxy-proline assays. Our results are consistent with these data. More specifically, we found a significant increase in the number of collagen fibers per unit of area (density), as determined by quantitative transmission electron microscopy, in Cav-1$^{-/-}$ mice skin as compared with wild-type controls. In addition, staining of the skin sections from mice with red picrosirius, visually demonstrated a significant accumulation of dermal collagen fibers in Cav-1$^{-/-}$ mice.

As mentioned above, skin from Cav-1$^{-/-}$ mice exhibits an abnormal overall organization and content of the collagen fibril network, and these characteristics should directly correlate with skin strength.[10,11,31] When we examined the bio-mechanical properties of the skin of Cav-1 null mice, we found an increase in skin strength in Cav-1 null mice, when compared with normal control mice. In addition, the skin of Cav-1$^{-/-}$ mice was also more resistant to percent elastic deformation caused by an applied stress, suggesting an increase in modulus of the skin material of these mice. Increases in skin strength and stiffness have been reported to be characteristics of fibrotic tissues, including Ssc skin.[12,43]

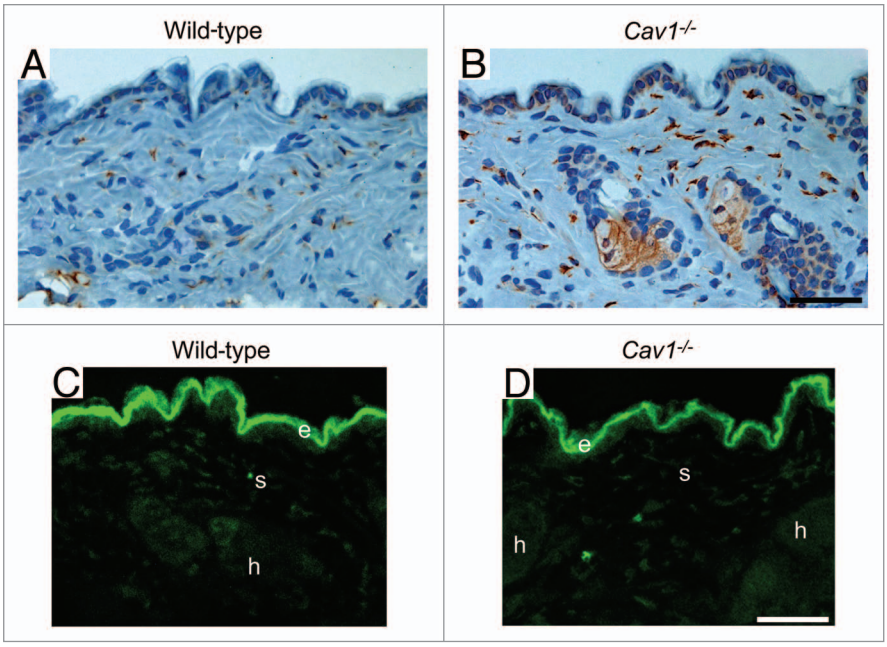

Figure 4. Cav-1$^{-/-}$ mice exhibit a net change in collagen synthesis. (A and B) Prolyl-4-hydroxylase (P4HB) expression in the skin from wild-type (A) and Cav-1$^{-/-}$ (B) mice. P4HB is a key enzyme in collagen biosynthesis that catalyzes the 4-hydroxylation of prolyl residues. Immuno-staining indicates positive labeling of the cells expressing P4HB. Representative images are shown from three animals per group. Note that the dermis of Cav-1$^{-/-}$ mice contains an increased number of P4HB positive cells. In addition, the P4HB positive cells in Cav-1$^{-/-}$ mice exhibited a marked increased expression of this enzyme. (C and D) In situ collagenase activity was determined using DQ-collagen type I, as substrate in skin from wild-type (B) and Cav-1$^{-/-}$ mice (C). Multiple cryostat sections of the skin from these animals were incubated overnight with DQ-Collagen type I, dissolved in LGT-agarose. Fluorescence due to collagenase activity (green) was found in the epidermis (e), stromal cells of the dermis (s) and in hair follicles (h). Note that we observed similar collagenase activity in the skin from both wild-type and Cav-1$^{-/-}$ mice. Take together, this data suggest that the skin from Cav-1$^{-/-}$ mice may displays a net increase in collagen synthesis and/or accumulation. Scale bar = 50 microns.

Therefore, our data suggest that the downregulation of Cav-1 reported in skin and fibroblasts from SSc patients,[19] may result in abnormal collagen fiber diameters and consequently increased tensile strength and modulus of the skin of these patients.

To explore collagenase activity in the skin of mice from wild-type and Cav-1$^{-/-}$ mice, we incubated skin sections with DQ-collagen type I. Using this approach, similar amounts of collagen type I were degraded by both Cav-1$^{-/-}$ and wild-type mice. Previous studies have shown that Cav-1 null skin fibroblasts exhibit decreased expression of MMP-3,[19] and skin from SSc patients contains a reduced total collagenase activity.[12] These data are not contradictory with the results obtained in here, as we determined the collagenase activity only of collagen type-I, whose degradation is mainly performed by MMP-8 and MMP-13. Therefore, it is possible that the skin from Cav-1 null mice may display attenuated activity for other MMPs, such as MMP-3. In summary, we observed increased P4HB expression in the skin of Cav-1$^{-/-}$ mice, but unchanged levels of collagenase type-I activity. Thus, our results support the concept that the dermis of Cav-1$^{-/-}$ mice exhibits a net increase in the synthesis of collagen, leading to the accumulation of this ECM component, which is a key hallmark of SSc.

Skin specimens from patients with SSc are also characterized by increased numbers of myo-fibroblasts,[44] which are considered to be "activated" fibroblasts that express alpha-smooth muscle actin (α-SMA) and possess high synthetic capacity for ECM proteins, including collagen and fibronectin, as well as the fibrogenic cytokines and chemokines.[6] Furthermore, Kissin et al. reported that the content of myo-fibroblasts in skin directly correlates as a clinical measure of disease activity and suggested that the quantification of myo-fibroblasts may be a useful outcome measure in clinical studies of SSc. In the present study, we observed an increased content of myo-fibroblasts in the dermis of Cav-1 null mice as compared with normal wild-type controls. These data are in agreement with the previous work from Del Galdo et al.[19] where they found that skin fibroblasts isolated from Cav-1$^{-/-}$ mice express higher levels of α-SMA, suggesting that skin Cav-1$^{-/-}$ fibroblasts take on a myo-fibroblastic phenotype. In support of increased myo-fibroblasts in the dermis of Cav-1$^{-/-}$ mice, we also observed an increase in the fibronectin content of the skin of these mice. Furthermore, fibronectin is highly expressed by myo-fibroblasts isolated from the dermis of scleroderma patients.[33,34]

The skin of patients in early stages of SSc is characterized by microvasculature and immunologic abnormalities.[1] In this study, we observed that skin from Cav-1$^{-/-}$ recapitulates some of these characteristics. In particular, we find an increased accumulation of dermal collagen fibers stained with picrosiruis red, suggesting sub-endothelial fibrosis as observed in patients with SSc. Furthermore, we observed an increase number of macrophages and mast cell infiltration in the skin from Cav-1$^{-/-}$ mice. The content of macrophages and mast cells is increased in the early stages of Ssc, suggesting that these inflammatory cells play a pivotal role in the progression of fibrotic disease.[13,14]

Transcriptional profiling of Cav-1$^{-/-}$ stromal cells directly supported an association with oxidative stress, mitochondrial dysfunction and autophagy/mitophagy.[25] Thus, we have proposed that defective mitochondria are removed from Cav-1$^{-/-}$ stromal cells by autophagy/mitophagy inducing a switch towards aerobic glycolysis.[46] In support of this notion, metabolic restriction with mitochondrial (complex I) and glycolysis inhibitors was synthetically lethal with a Cav-1$^{-/-}$ deficiency in mice.[46] Similarly, herein, we also found that stromal cells from the dermis of Cav-1$^{-/-}$ mice exhibit increased autophagy/mitophagy activity, suggesting that their main metabolism is that of aerobic glycolysis. Interestingly, keloid "scar" fibroblasts, which share many characteristics with SSc fibroblasts, are known to use aerobic glycolysis as their primary energy source.[47] Thus, it is tempting to propose that a

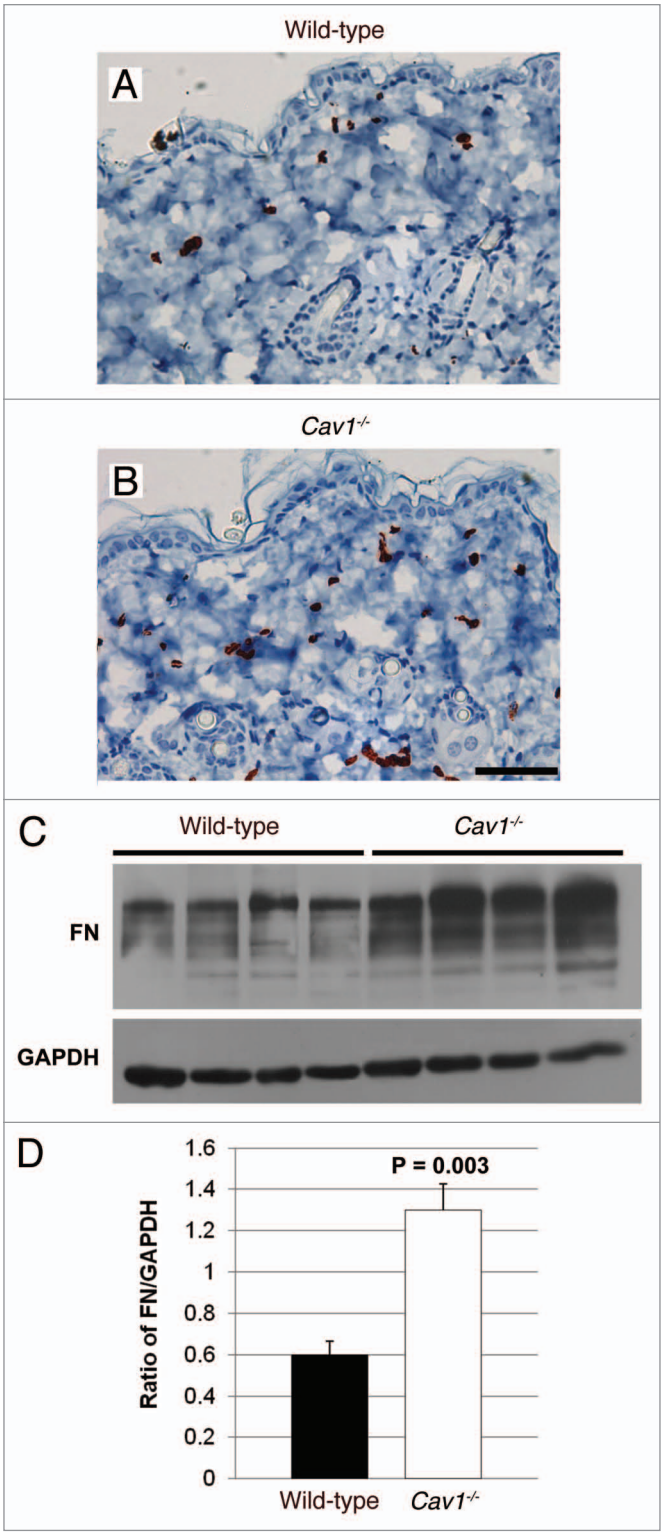

Figure 5. Immunohistochemical detection of myo-fibroblasts in the skin of wild-type and Cav-1$^{-/-}$ mice. Skin sections from wild-type (A) and Cav-1$^{-/-}$ (B) mice were stained with α-SMA, a myo-fibroblast cell marker. Immuno-staining indicates positive labeling of myo-fibroblasts. Representative images are shown from three animals per group. Note that an increased number of α-SMA positive cells was observed in the dermis of Cav-1$^{-/-}$ mice, as compared to normal wild-type skin. (C) Analysis of fibronectin expression in the skin of wild-type and Cav-1$^{-/-}$ mice. Western blots of total protein extracted from wild-type and Cav-1$^{-/-}$ mice shows the expression of fibronectin (FN) and the loading control glyceraldehydes-3-phosphate dehydrogenase (GAPDH). (D) Quantification of fibronectin expression in the in the skin of wild-type and Cav-1$^{-/-}$ mice. Intensity of the western blot bands for fibronectin and GAPDH were quantified using NIH Image J. Note that a significant increased in fibronectin expression was observed in the Cav-1$^{-/-}$ skin, as compared to normal wild-type mouse skin. Results are indicated as the mean ± SEM. p values are indicated in the graphs, as determined by the Student's t-test. Scale bar = 50 microns.

greater reliance on glycolysis in skin Cav-1$^{-/-}$ fibroblasts confers the capacity to proliferate and survive in a hypoxic environment. Therefore, glycolytic inhibitors may be a new therapeutic strategy for preventing fibrosis in scleroderma patients. In support of this notion, Bonnet and colleagues have shown that therapy with dichloroacetate (DCA), a glycolytic inhibitor that induces a switch towards oxidative metabolism, was sufficient to reverse the aerobic glycolysis (Warburg effect) of pulmonary smooth muscle cells, reducing fibrosis and increasing survival of pulmonary alterial hypertension (PAH) in fawn-hooded rats.[48]

Research into SSc has been hampered by its low incidence, its heterogeneity and the lack of mouse models that accurately recapitulate the disease. Here, we directly showed that the skin from Cav-1 null mice shares many physical and functional characteristics with skin from SSc patients, including increased myofibroblast content, collagen density, infiltration with immune cells and fibrotic vessels, as well as increased tensile strength and modulus. Thus, our data suggest that skin of Cav-1 null mice may be a new pre-clinical model of SSc. Therefore, the Cav-1 null mice may also serve as a promising tool for development of new therapies for halting the progression of fibrosis in SSc patients.

Materials and Methods

Animals. Gene-targeted mice deficient in Caveolin-1 (Cav-1$^{-/-}$) were generated and genotyped as previously described in reference 17. All wild-type control and Cav-1$^{-/-}$ mice were maintained on the C57BL/6 genetic background. For most of the studies, 8 to 10 week-old virgin female mice were used, unless stated otherwise. Animal protocols used for this study were pre-approved by the *Institutional Animal Care and Use Committee* (IACUC).

Morphological analysis. Skin and tail tendons from age-matched wild-type and Cav-1$^{-/-}$ mice were collected, cut in small segments and immediately fixed in 2% glutaradehyde in 0.2 M phosphate buffer for 24 h at 4°C. The specimens were then post-fixed in 1% osmium tetroxide in 0.2 M phosphate buffer, dehydrated in graded alcohols and infiltrated with mixtures of embedding medium and alcohol. Then, the tissue fragments were embedded in Spurr's embedding medium and polymerized overnight at 80°C. Semi-thin (1 μm) and thin (100 nm) sections were cut on a Reichert Ultracut S ultramicrotome, using glass knives and diamond knife, respectively. The semi-thin sections were transferred to glass microscope slides, stained with Toluidine Blue O stain and reviewed using a light microscope. The thin sections were collected onto copper grids and stained with uranyl acetate and lead citrate. The stained thin sections were evaluated

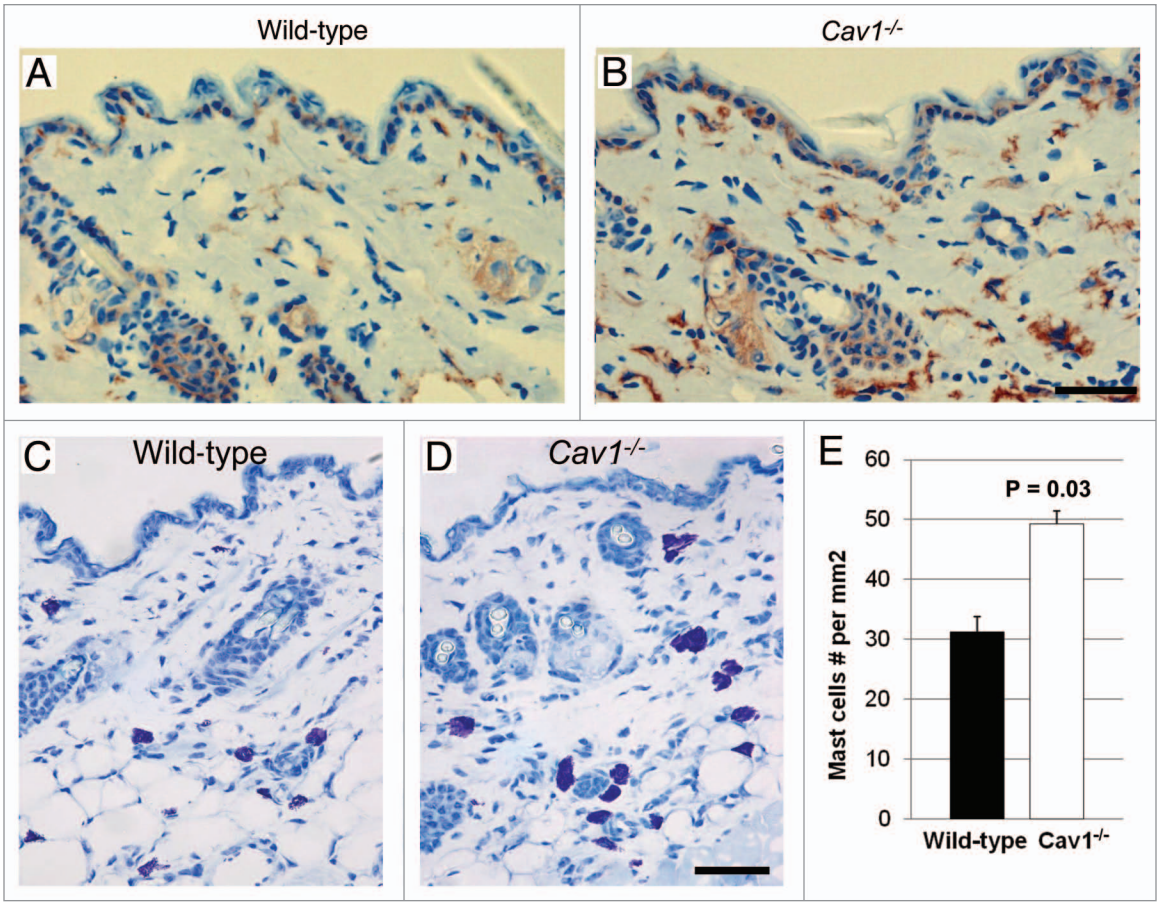

Figure 6. Inflammatory cell content of the skin in wild-type and Cav-1$^{-/-}$ mice. (A and B) Frozen sections from the skin were stained with the F4/80 antibody, a macrophage cell marker, to evaluate macrophage infiltration in the dermis of wild-type (A) and Cav-1$^{-/-}$ mice (B). Immuno-staining indicates positive labeling of macrophages. (C and D) Histochemical staining to detect mast cells. Using this approach mast cells stain purple. Scale bar = 50 microns. (E) Quantification of mast cells in the skin from wild-type and Cav-1$^{-/-}$ mice. The number of mast cells was determined in five equal areas of skin (n = 5), from the sub-endothelium to the muscle. Note that increased infiltration of macrophages and mast cells was observed in the dermis of Cav-1$^{-/-}$ mice, as compared with normal wild-type dermis. Results are indicated as the mean ± SEM. p values are indicated in the graphs, as determined by the Student's t-test.

and photographed, utilizing a JEOL 100CX II electron microscope. The resulting negative images were scanned using a computer system and Adobe Photoshop. We designed an algorithm to automatically count the collagen fibrils from the scanned electron microscopy images using ImageJ (see **Sup. Fig. 1**). Briefly, the images were median filtered to remove speckle noise, and then thresholded using "Maximum Entropy Thresholding."[26] Objects were then split using a watershed algorithm.[27] Image J's particle analysis was then used to count and measure fiber diameters, area and area fractions. Resulting data was processed using SigmaPlot, to generate histograms of comparison data. The degree of significance between control and experimental groups was determined with the Mann-Whitney Rank Sum Test using SigmaPlot version 11.0 and SigmaStat package for Windows version 3.1 (Instat Software Inc., Port Richmond, CA). Statistical significance was achieved when p values were < 0.05.

Picrosirius red staining. Paraffin-embedded skin sections were de-waxed and rehydrated through a graded series of ethanol. The nuclei were then stained with Weigert's haematoxylin for 8 min. After washing with water, the slides were incubated in a picric acid-saturated solution containing 0.1% picrosirius red (Sigma) for 1 hour. Then, the slides were washed twice with 0.5% acetic acid. Finally, the sections were alcohol dehydrated and mounted. Images were acquired using a LEICA DM5500B microscope with Leica Application Suite, under polarizing light (Leica Microsystems, Inc.). All the images were analyzed using the software mentioned above, along with Adobe Photoshop CS3 (Adobe Systems, San Jose, CA).

Biomechanical test of skin tensile strength. Five age-matched wild-type and five Cav-1$^{-/-}$ mice were sacrificed at 2 months of age. Skin was dissected posteriorly off the dorsum of all mice. A dumbbell stamping fixture was used to obtain a consistent sample for mechanical testing from the same part of the dorsum. A gauge length was demarcated using Verhoeff's stain, for later use in calculation of local tissue strain[28] using texture correlation. Cross-sectional area was measured within the gauge length using a CCD laser-based device, as described previously in reference 29. Briefly, using position data from a linear variable differential transformer (LVDT) in the transverse direction in addition to thickness data from the laser, mean cross-sectional area was

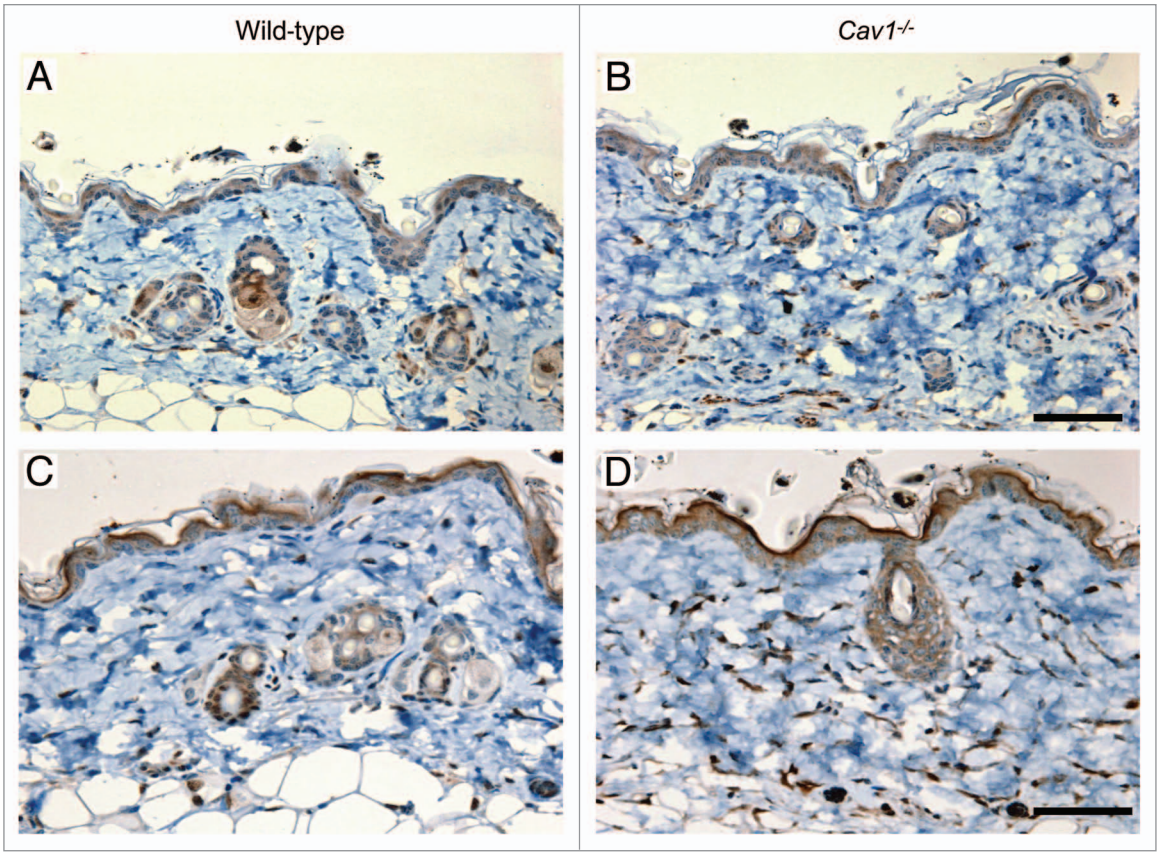

Figure 7. Autophagy/mitophagy in stromal cells from the dermis of wild-type and Cav-1$^{-/-}$ mice. Paraffin-embedded sections from the skin were stained with a LC3 antibody, to evaluate the degree of autophagy in stromal cells in the dermis of wild-type (A) and Cav-1$^{-/-}$ mice (B). Note that an increased number of stromal cells are positive for LC3 in the dermis of Cav-1$^{-/-}$ mice, in comparison to wild-type mice. The skin sections of these two groups were also stained with BNIP3L, a mitophagy marker. A marked increased in the number of dermal stromal cells that are positive for BNIP3L was observed in Cav-1$^{-/-}$ mice (D), in comparison with wild-type mice (C).

calculated by using the axial LVDT position data to interpolate between each of five transverse passes across the specimen width, using custom software. Each specimen end was fixed between two layers of sandpaper, using a cyanoacrylate adhesive to prevent slipping. Sample ends were clamped in custom test fixtures and tensile tested in an Instron 5543 (Instron Corp., Norwood, MA) mechanical test frame. All specimens were subjected to the following testing protocol, as performed previously in reference 30, while submerged in 37°C PBS: preload to 0.03 N, hold for 120 s and constant ramp to failure at a rate of 1.67%/s. Maximum stress was calculated as the failure point in the load response divided by the measured cross-sectional area within the gauge length. Young's modulus was calculated as the slope of the stress-strain curve within the elastic region of the ramp to failure. Differences in the means between wild-type and Cav-1$^{-/-}$ skin were compared using the Student's t-test, with significance set at $p \leq 0.05$.

Immuno-histochemistry. Skin from wild-type and Cav-1$^{-/-}$ mice was harvested and frozen in OCT compound using liquid nitrogen for frozen section analyses or fixed in 10% phosphate-buffered formalin for paraffin embedding. For immunohistochemistry using paraffin-embedded sections (4–6 μm), slides were incubated at 55°C for 30 min, de-waxed with xylene and rehydrated through a graded series of ethanol. Antigen retrieval was performed in 10 mM sodium citrate, pH 6 for 10 min using a pressure cooker. After cooling, the sections were blocked with 3% hydrogen peroxide followed by incubation with 10% goat serum/PBS for 1 h at RT. Anti-mouse alpha-smooth muscle actin (α-SMA, 1:100, Dako, Carpinteria, CA) was applied overnight at 4°C. The next day, the slides were washed twice with PBS (for 5 min each) and incubated with a biotinylated goat anti-mouse antibody (1:500, Vector Labs, Burlingame, CA) for 30 min at RT. Slides were then washed and incubated with streptavidin-horseradish peroxidase solution for 30 min at RT. Immuno-reactivity was revealed using an ImmPACT NovaRED peroxidase substrate kit (Vector), per the manufacturer's instructions. Finally, the sections were counter-stained with hematoxylin for 5–10 sec, air-dried and mounted with coverslips. For immunohistochemistry using frozen sections (6 μm), the slides were fixed with 4% para-formaldehyde in PBS for 10 min at 4°C and washed three times with PBS. After blocking with 10% rabbit (F4/80) or goat (P4HB) serum for 1 h at RT, tissue sections were incubated with polyclonal anti-rabbit prolyl-4 hydroxylase beta (P4HB, 1:1,000, *Proteintech* Group, Inc.) or rat monoclonal anti-mouse F4/80 (1:100, *Fitzgerald Industries* International) overnight at 4°C. The next day, the sections were

washed with PBS and incubated with a biotinylated rabbit anti-rat IgG (F4/80) or a goat anti-rabbit (P4HB) IgG (Vector). After washing, peroxidase activity was blocked with 0.3% H_2O_2/PBS for 10 min at RT. Subsequent steps were as described for paraffin-embedded sections.

In situ collagenase activity. Collagenase activity was examined in unfixed cryostat sections of skin from wild-type and Cav-1$^{-/-}$ mice using DQ-Collagen type I, as a substrate (EnzChek; Molecular Probes, Eugene, OR). DQ-Collagen type I (1 mg/ml) was dissolved 1:10 diluted in 1% (w/v) low gelling temperature agarose (LGT) (Sigma) in PBS. The mixture was put on the top of the sections and covered with a coverslip. Then the agarose was gelled at 4°C and sections were incubated overnight at RT in the dark. Fluorescence FITC due to collagenase activity was observed with a confocal microscope. To evaluate the tissue autofluorescence, several skin sections were incubated with agarose in absence of DQ-Collagen type I. Images were collected with a Zeiss LSM510 meta confocal system using a 488 nm Argon excitation laser and a detector range of 505–550 nm.

Immunoblotting. Mice were sacrificed and skin samples were surgically removed and homogenized in RIPA buffer (150 mmol/L NaCl, 0.5% deoxycholate, 1% Triton X-100, 0.1% sodium dodecyl sulfate (SDS) and 50 mM Tris-HCl, pH 7.5) containing protease and phosphatase inhibitors (Roche Applied Science, Indianapolis, IN). The protein concentration of the lysates was determined using BCA assay (Pierce) according the manufacturer's instructions. Equal amounts of protein (50 μg) were separated by sodium dodecyl sulfate-polyacrylamide gel electrophoresis (10% acryalmide) and transferred to a nitrocellulose membrane. Membranes were blocked with TBST (20 mM Tris-HCl pH 7.6, 137 mM NaCl, 0.1% Tween 20) containing 5% non fat dry milk for 4 h at RT. Then, membranes were incubated with polyclonal anti-fibronectin (1:1,000, Abcam) overnight at 4°C or monoclonal anti-mouse GAPDH antibody (1:5,000, Chemicon International Inc.) for 1 h at RT. Blots were then washed three times with TBST for 10 min each and incubated with HRP conjugated goat anti-rabbit antibody (1:5,000, BD Biosciences) for 40 min at RT. After washing three times with TBST for 10 min each, the signal was detected using an ECL detection kit (Pierce). Quantification of the bands intensity was performed using NIH ImageJ software. Differences in the means between wild-type and Cav-1$^{-/-}$ were compared using the Student's t-test, with significance set at $p \leq 0.05$.

Mast cell staining and quantification. Frozen skin sections from wild-type and Cav-1$^{-/-}$ mice were thawed and fixed with 4% paraformaldehyde in PBS for 10 min. Then, the sections were washed twice with PBS, rinsed in water and stained with 1% Toluidine Blue O in isopropanol for 30 sec. Finally, the sections were washed in water to remove excess color, air dried and placed in xylene for 5 min and coverslipped with permount. Mast cells were counted under 20X magnification of a light microscope equipped with a 0.5 x 0.5-mm grid. The number of mast cells was counted in five grid fields of the skin (five animals per group) from the sub-endothelium to the muscle. Statistical analyses were performed using the Student's t-test.

Acknowledgments

M.P.L. and his laboratory were supported by grants from the NIH/NCI (R01-CA-080250; R01-CA-098779; R01-CA-120876; R01-AR-055660), and the Susan G. Komen Breast Cancer Foundation. F.S. was supported by grants from the W.W. Smith Charitable Trust, the Breast Cancer Alliance (BCA), and a Research Scholar Grant from the American Cancer Society (ACS). Funds were also contributed by the Margaret Q. Landenberger Research Foundation (to M.P.L.). R.V.I. was supported by NIH grants RO1 CA39481, RO1 CA47282 and RO1 CA120975. This work was also supported, in part, by National Institutes of Health Grant AR050950 from NIAMS (to L.J.S.), supporting the Penn Center for Musculoskeletal Disorders.

Note

Supplemental materials can be found at:
www.landesbioscience.com/journals/cc/article/16227

References

1. Jimenez SA, Derk CT. Following the molecular pathways toward an understanding of the pathogenesis of systemic sclerosis. Ann Intern Med 2004; 140:37-50.
2. LeRoy EC. Increased collagen synthesis by scleroderma skin fibroblasts in vitro: A possible defect in the regulation or activation of the scleroderma fibroblast. J Clin Invest 1974; 54:880-9.
3. Jimenez SA, Feldman G, Bashey RI, Bienkowski R, Rosenbloom J. Co-ordinate increase in the expression of type I and type III collagen genes in progressive systemic sclerosis fibroblasts. Biochem J 1986; 237:837-43.
4. Jimenez SA, Bashey RI. Collagen synthesis by scleroderma fibroblasts in culture. Arthritis Rheum 1977; 20:902-3.
5. Takeda K, Hatamochi A, Ueki H, Nakata M, Oishi Y. Decreased collagenase expression in cultured systemic sclerosis fibroblasts. J Invest Dermatol 1994; 103:359-63.
6. Gabbiani G. The myofibroblast in wound healing and fibrocontractive diseases. J Pathol 2003; 200:500-3.
7. Jimenez SA, Hitraya E, Varga J. Pathogenesis of scleroderma. Collagen. Rheum Dis Clin North Am 1996; 22:647-74.
8. Lakos G, Takagawa S, Chen SJ, Ferreira AM, Han G, Masuda K, et al. Targeted disruption of TGF{beta}/Smad3 signaling modulates skin fibrosis in a mouse model of scleroderma. Am J Pathol 2004; 165:203-17.
9. Fleischmajer R, Gay S, Meigel WN, Perlish JS. Collagen in the cellular and fibrotic stages of scleroderma. Arthritis Rheum 1978; 21:418-28.
10. Danielson KG, Baribault H, Holmes DF, Graham H, Kadler KE, Iozzo RV. Targeted disruption of decorin leads to abnormal collagen fibril morphology and skin fragility. J Cell Biol 1997; 136:729-43.
11. Dombi GW, Haut RC, Sullivan WG. Correlation of high-speed tensile strength with collagen content in control and lathyritic rat skin. J Surg Res 1993; 54:21-8.
12. Brady AH. Collagenase in scleroderma. J Clin Invest 1975; 56:1175-80.
13. Jimenez SA. Cellular immune dysfunction and the pathogenesis of scleroderma. Semin Arthritis Rheum 1983; 13:104-13.
14. Kraling BM, Maul GG, Jimenez SA. Mononuclear cellular infiltrates in clinically involved skin from patients with systemic sclerosis of recent onset predominantly consist of monocytes/macrophages. Pathobiology 1995; 63:48-56.
15. Severs NJ. Caveolae: Static inpocketings of the plasma membrane, dynamic vesicles or plain artifact? J Cell Sci 1988; 90:341-8.
16. Razani B, Woodman SE, Lisanti MP. Caveolae: From cell biology to animal physiology. Pharmacol Rev 2002; 54:431-67.
17. Razani B, Engelman JA, Wang XB, Schubert W, Zhang XL, Marks CB, et al. Caveolin-1 null mice are viable but show evidence of hyperproliferative and vascular abnormalities. J Biol Chem 2001; 276:38121-38.
18. Drab M, Verkade P, Elger M, Kasper M, Lohn M, Lauterbach B, et al. Loss of caveolae, vascular dysfunction and pulmonary defects in caveolin-1 gene-disrupted mice. Science 2001; 293:2449-52.
19. Del Galdo F, Sotgia F, de Almeida CJ, Jasmin JF, Musick M, Lisanti MP, et al. Decreased expression of caveolin 1 in patients with systemic sclerosis: crucial role in the pathogenesis of tissue fibrosis. Arthritis Rheum 2008; 58:2854-65.
20. Tourkina E, Gooz P, Pannu J, Bonner M, Scholz D, Hacker S, et al. Opposing effects of protein kinase Calpha and protein kinase Cepsilon on collagen expression by human lung fibroblasts are mediated via MEK/ERK and caveolin-1 signaling. J Biol Chem 2005; 280:13879-87.

21. Wang XM, Zhang Y, Kim HP, Zhou Z, Feghali-Bostwick CA, Liu F, et al. Caveolin-1: A critical regulator of lung fibrosis in idiopathic pulmonary fibrosis. J Exp Med 2006; 203:2895-906.
22. Martinez-Outschoorn UE, Trimmer C, Lin Z, Whitaker-Menezes D, Chiavarina B, Zhou J, et al. Autophagy in cancer associated fibroblasts promotes tumor cell survival: Role of hypoxia, HIF1 induction and NFkappaB activation in the tumor stromal microenvironment. Cell Cycle 2010; 9:3515-33.
23. Hong KH, Yoo SA, Kang SS, Choi JJ, Kim WU, Cho CS. Hypoxia induces expression of connective tissue growth factor in scleroderma skin fibroblasts. Clin Exp Immunol 2006; 146:362-70.
24. Sambo P, Baroni SS, Luchetti M, Paroncini P, Dusi S, Orlandini G, et al. Oxidative stress in scleroderma: Maintenance of scleroderma fibroblast phenotype by the constitutive upregulation of reactive oxygen species generation through the NADPH oxidase complex pathway. Arthritis Rheum 2001; 44:2653-64.
25. Pavlides S, Tsirigos A, Migneco G, Whitaker-Menezes D, Chiavarina B, Flomenberg N, et al. The autophagic tumor stroma model of cancer: Role of oxidative stress and ketone production in fueling tumor cell metabolism. Cell Cycle 2010; 9:3485-505.
26. Sahoo PK, Soltani S, Wong AKC, Chen YC. A survey of thresholding techniques. Comput Vision Graph Image Process 1988; 41:233-60.
27. Beucher S, Lantuéjoul C. Use of watersheds in contour detection. In *International workshop on image processing, real-time edge and motion detection*. France 1979.
28. Derwin KA, Soslowsky LJ, Green WD, Elder SH. A new optical system for the determination of deformations and strains: calibration characteristics and experimental results. J Biomech 1994; 27:1277-85.
29. Favata M. Scarless Healing in the fetus: Implications and strategies for postnatal tendon repair. Ph.D., Dissertation Philadelphia University of Pennsylvania 2006.
30. Christner PJ, Gentiletti J, Peters J, Ball ST, Yamauchi M, Atsawasuwan P, et al. Collagen dysregulation in the dermis of the Sagg/+ mouse: A loose skin model. J Invest Dermatol 2006; 126:595-602.
31. Fry P, Harkness ML, Harkness RD. Mechanical Properties of the collagenous framework of skin in rats of different ages. Am J Physiol 1964; 206:1425-9.
32. Keiser HR, Stein HD, Sjoerdsma A. Increased protocollagen proline hydroxylase activity in sclerodermatous skin. Arch Dermatol 1971; 104:57-60.
33. Fleischmajer R, Perlish JS, Krieg T, Timpl R. Variability in collagen and fibronectin synthesis by scleroderma fibroblasts in primary culture. J Invest Dermatol 1981; 76:400-3.
34. Meyringer R, Neumann E, Judex M, Landthaler M, Kullmann F, Scholmerich Jr, et al. Analysis of gene expression patterns in systemic sclerosis fibroblasts using RNA arbitrarily primed-polymerase chain reaction for differential display. J Rheumatol 2007; 34:747-53.
35. Del Galdo F, Lisanti MP, Jimenez SA. Caveolin-1, transforming growth factor-beta receptor internalization and the pathogenesis of systemic sclerosis. Curr Opin Rheumatol 2008; 20:713-9.
36. Hayes RL, Rodnan GP. The ultrastructure of skin in progressive systemic sclerosis (scleroderma). I. Dermal collagen fibers. Am J Pathol 1971; 63:433-42.
37. Fleischmajer R, Damiano V, Nedwich A. Scleroderma and the subcutaneous tissue. Science 1971; 171:1019-21.
38. Rosenbloom J, Harsch M, Jimenez S. Hydroxyproline content determines the denaturation temperature of chick tendon collagen. Arch Biochem Biophys 1973; 158:478-84.
39. Walmsley AR, Batten MR, Lad U, Bulleid NJ. Intracellular retention of procollagen within the endoplasmic reticulum is mediated by prolyl 4-hydroxylase. J Biol Chem 1999; 274:14884-92.
40. Kawaguchi Y, Kitani A, Hara M, Harigai M, Hirose T, Suzuki K, et al. Cytokine regulation of prolyl-4-hydroxylase production in skin fibroblast cultures from patients with systemic sclerosis: contribution to collagen synthesis and fibrosis. J Rheumatol 1992; 19:1195-201.
41. Kawaguchi Y, Harigai M, Kitani A, Suzuki K, Kawakami M, Ishizuka T, et al. Effect of prolyl 4-hydroxylase inhibitor on fibroblast collagen production in vitro: An approach to the treatment of systemic sclerosis. J Rheumatol 1992; 19:1710-5.
42. Uitto J, Halme J, Hannuksela M, Peltokallio P, Kivirikko KI. Protocollagen proline hydroxylase activity in the skin of normal human subjects and of patients with scleroderma. Scand J Clin Lab Invest 1969; 23:241-7.
43. Knight LR, Smeathers JE, Isdale AH, Helliwell PS. Evaluating the cutaneous involvement in scleroderma: Torsional stiffness revisited. Rheumatology 2001; 40:128-32.
44. Sappino AP, Masouye I, Saurat JH, Gabbiani G. Smooth muscle differentiation in scleroderma fibroblastic cells. Am J Pathol 1990; 137:585-91.
45. Kissin EY, Merkel PA, Lafyatis R. Myofibroblasts and hyalinized collagen as markers of skin disease in systemic sclerosis. Arthritis Rheum 2006; 54:3655-60.
46. Pavlides S, Tsirigos A, Vera I, Flomenberg N, Frank PG, Casimiro MC, et al. Loss of stromal caveolin-1 leads to oxidative stress, mimics hypoxia and drives inflammation in the tumor microenvironment, conferring the "reverse Warburg effect": A transcriptional informatics analysis with validation. Cell Cycle 2010; 9.
47. Vincent AS, Phan TT, Mukhopadhyay A, Lim HY, Halliwell B, Wong KP. Human skin keloid fibroblasts display bioenergetics of cancer cells. J Invest Dermatol 2008; 128:702-9.
48. Bonnet S, Michelakis ED, Porter CJ, Andrade-Navarro MA, Thebaud B, Bonnet S, et al. An abnormal mitochondrial-hypoxia inducible factor-1{alpha}-Kv channel pathway disrupts oxygen sensing and triggers pulmonary arterial hypertension in fawn hooded rats: Similarities to human pulmonary arterial hypertension. Circulation 2006; 113:2630-41.